THE EFFECT OF DIGITAL AND PHYSICAL FILTERS ON IMAGE QUALITY FOR QUANTITATIVE Tc-99m SINGLE PHOTON EMISSION COMPUTED TOMOGRAPHY (SPECT)

BY

RUKIAH A. LATIFF

Thesis submitted in fulfillment of the
requirements for the degree
of Master of Science

MEI 2010

DEDICATIONS

This thesis is specially dedicated to:

My beloved husband, Norman Tasli b. Mohd. Razali
My sons, Nabil Rifqi & Najid Rifqi
My parents, Hj. A. Latiff dan Hjh. Hazanah

Thank you for your love, support and patience..
May God bless you all..

ACKNOWLEDGEMENTS

In the name of Allah, the most Generous and the most Merciful. All praise is due to Allah, for giving me strength and inspiration along this journey.

During this research project, there are several people involved directly and indirectly whom I wish to acknowledge in this section.

I would like to thank my supervisor, Prof. Dr. Ahmad b. Zakaria for his support, excellent guidance and supervision throughout the research project and during the writing of thesis. I wish to thank him for his trustee and confidence in me to carry out this project. His guidance is greatly appreciated.

I would like also to thank the staff of Department of Nuclear Medicine, Radiotherapy and Oncology especially Mr. Ismail, Mrs. Noraini and Mr. Nizam and the staff of School of Health Sciences especially Mr. Waidi who are very helpful by giving advice and comments during this study. Not to forget my friends Ku, Eza, Syikin, Fini, Ijan and Zura who are very helpful .

Finally, my deepest appreciation will be to my beloved husband, Norman Tasli b. Mohd. Razali for his greatest support, patience, love and encouragement. My appreciation also goes to my beloved son Nabil Rifqi, his mischievousness had always cheered me. A special thanks to my parents, Hj. A. Latiff and Hjh. Hazanah and my parents in-law Hj. Mohd. Razali and Hjh. Tasliah for their understanding and support.

TABLE OF CONTENTS

Page

AKNOWLEDGEMENT iii

TABLE OF CONTENTS iv

LIST OF TABLES viii

LIST OF FIGURES ix

LIST OF PLATES xvi

LIST OF ABBREVIATIONS xvii

LIST OF SYMBOLS xix

ABSTRAK xx

ABSTRACT xxii

CHAPTER I : INTRODUCTION

1.1 Single Photon Emission Computed Tomography (SPECT) 1

1.2 Principle of gamma camera 2

1.3 SPECT image reconstruction 3

- 1.3.1 Simple backprojection 3
- 1.3.2 Filtered backprojection (FBP) 4

1.4 SPECT reconstruction filters 5

- 1.4.1 Nyquist frequency 9

1.5 Literature review

- 1.5.1 SPECT quantittation 10
- 1.5.2 Image segmentation and boundary detection 12
- 1.5.3 Attenuation correction 14
- 1.5.4 Scattered radiation correction 15

1.6 Aim of the study 25

- 1.6.1 Objectives of the study 25

CHAPTER II : MATERIALS AND METHODS

2.1 Study design 26

2.2 Materials 29

- 2.2.1 Gamma camera 30
- 2.2.2 Image acquisition workstation 30
- 2.2.3 Pegasys image processing & display workstation 30
- 2.2.4 Collimator 31
- 2.2.5 Cylindrical phantoms 32
- 2.2.6 Cylindrical water tank phantom 33
- 2.2.7 Radionuclide 34
- 2.2.8 Physical filters 35

2.3 Methodology

- 2.3.1 Investigating the effect of mathematical filters on the count of reconstructed images 36
  - 2.3.1.1 Phantoms preparation 36
  - 2.3.1.2 SPECT data acquisition 36
  - 2.3.1.3 Image processing 37
    - 2.3.1.3.1 Image reconstruction 37
    - 2.3.1.3.2 Total count 39
- 2.3.2 Investigating the effect of mathematical filters on image quality scanning in water and radioactive medium 39
  - 2.3.2.1 Phantoms preparation 40
  - 2.3.2.2 SPECT data acquisition 40
  - 2.3.2.3 Image processing 41
    - 2.3.2.3.1 Image reconstruction 41
    - 2.3.2.3.2 Contrast image 41
    - 2.3.2.3.3 Signal-noise ratio (SNR) 42

2.3.3 Investigating the effect of physical filters on image quality for quantification 43

2.3.3.1 Selection of physical filters thickness 43

2.3.3.2 Phantoms preparation 43

2.3.3.3 SPECT data acquisition 44

2.3.3.4 Image processing 44

2.3.3.4.1 Image reconstruction 44

2.3.3.4.2 Contrast image 45

2.3.3.4.3 Signal-noise ratio (SNR) 45

2.3.4 Estimating the volume of the objects of various sizes and total activity present inside the object 45

2.3.4.1 Volume determination 45

2.3.4.2 Total activity determination 46

CHAPTER III: RESULTS

3.1 The effect of mathematical filters on the count of reconstructed images 48

3.2 The effect of mathematical filters on image quality scanning in water and radioactive medium 59

3.2.1 Contrast and signal-noise ratio of phantoms in water 59

3.2.2 Contrast and signal-noise ratio of phantoms in radioactive medium 83

3.3 The effect of physical filters on image quality for quantification 109

3.3.1 Selection of physical filters thickness 109

3.3.2 Effect of physical filters on total count for different size of phantoms 110

3.3.3 Contrast 111

3.3.4 Signal-noise ratio 112

3.4 Estimating the volume of the objects and total activity presents inside the objects 116

3.4.1 Volume estimation 116

3.4.2 Total activity estimation 118

CHAPTER IV: DISCUSSIONS

4.1. The effect of mathematical filters on the count of reconstructed images 120

4.2. The effect of mathematical filters on image quality scanning in water and radioactive medium 122

4.3. The effect of physical filters on image quality for quantification 127

4.3.1. Effect of physical filters on total count 127

4.3.2. Effect of physical filters on image quality 129

4.4. Estimating the volume of the objects and the activity present inside the objects 131

CHAPTER V: CONCLUSION 134

REFERENCES 136

APPENDICES 142

LIST OF TABLES

Page

Table 3.1 Comparison of the mean count relative errors (%) without physical filters and with physical filters. 110

Table 3.2 Percentage of count difference between no physical filter and with physical filter. 110

Table 3.3 Contrast without and with physical filters 112

Table 3.4 SNR without and with physical filters 113

Table 3.5 Comparison of the mean relative errors (%) and standard deviation between the true and the calculated volumes without physical filters and with physical filters 116

Table 3.6 Comparison of the mean relative errors (%) and standard deviation between the true and the total activities without physical filters and with physical filters 118

LIST OF FIGURES

		Page
Figure 1.1	A schematic diagram showing the detection of photons emitted from the radionuclide in the body	1
Figure 1.2	Schematic representation showing a conversion of γ-rays to voltage signals in gamma camera system	3
Figure 1.3	Basic principle of image reconstruction by backprojection technique	4
Figure 1.4	Ramp filter function	6
Figure 1.5	The ramp filter removes background noise at low frequency and accept useful image data and high noise.	6
Figure 1.6	Different windows suppress the high frequencies with a cut-off Nyquist frequency of 0.5 cycle/pixel	7
Figure 1.7	Different windows by multiplying respective filters with the Ramp filter.	8
Figure 1.8	Butterworth filter with different orders, n and cutoff frequencies, v_c	9
Figure 1.9	The figure shows the different primary and scatter spectrum energy of different radioactive	16
Figure 1.10	C_{total} is the main window while C_{left} and C_{right} are the subwindows located at the end of the main window	19
Figure 1.11	Energy spectrum showing location of lower (L) and upper (U) windows used in dual-photopeak window	19
Figure 1.12	a) Placement of windows on the photopeak when no scatter is present. b) Contribution made by scattered radiation to the photopeak energy windows.	20
Figure 1.13	Energy spectrum of ^{99m}Tc in the scattering material with (dashed line) and without (dotted line) filter normalized to the same peak.	23
Figure 1.14	^{99m}Tc spectrum from patient	24

Figure 2.1 Flowchart of the study 28

Figure 2.2 Image display for SPECT Reconstruction application 38

Figure 2.3 Image display to obtain total count 39

Figure 2.4 An information shown in Count Profile display 46

Figure 3.1 Percentage reduction of image count after reconstruction using Ramp filter 48

Figure 3.2 Percentage reduction of image count after reconstruction using Gaussian filter order 7 with 5 different cof for various size of phantoms. 49

Figure 3.3 Percentage reduction of image count after reconstruction using Gaussian filter order 14 with 5 different cof of various size of phantoms. 50

Figure 3.4 Percentage reduction of image count after reconstruction using Gaussian filter order 21 with 5 different cof of various size of phantoms. 50

Figure 3.5 Percentage reduction of image count after reconstruction using Gaussian filter order 28 with 5 different cof of various size of phantoms. 51

Figure 3.6 Average percentage count reduction of image reconstruction using Gaussian filter with different cof and order. 52

Figure 3.7 Percentage of image count difference between before and after reconstructed using Butterworth filter order 8 with 5 different cof of various size of phantoms. 53

Figure 3.8 Percentage of image count difference between before and after reconstructed using Butterworth filter order 16 with 5 different cof of various size of phantoms. 53

Figure 3.9 Percentage of image count difference between before and after reconstruction using Butterworth filter order 24 with 5 different cof for various sixes of phantoms. 54

Figure 3.10 Percentage of image count difference between before and after reconstruction using Butterworth filter order 32 with 5 different cof of various size of phantoms. 54

Figure 3.11 Average percentage of image count difference reconstruction using Butterworth filters with different cof and orders. 55

Figure 3.12 Percentage of image count difference between before and after reconstruction using Parzen filter for various size of phantoms. 56

Figure 3.13 Percentage of image count difference between before and after reconstruction using Hamming filter for various size of phantoms. 57

Figure 3.14 Percentage of image count difference between before and after reconstruction using Hanning filter for various size of phantoms. 58

Figure 3.15 Percentage reduction of count image after reconstructed using Butterworth filter order 5, cof 0.35 Nq. 59

Figure 3.16 Contrast for Ramp filter in water 60

Figure 3.17 SNR for Ramp filter in water 60

Figure 3.18 Transverse image when reconstructed using Ramp filter scanning in water 61

Figure 3.19 Contrast obtained by Parzen filter with different cof in water. 61

Figure 3.20 SNR obtained by Parzen filter with different cof in water. 62

Figure 3.21 Transverse image when reconstructed using Parzen filter scanning in water. 62

Figure 3.22 Contrast obtained by Hamming filter with different cof in water. 63

Figure 3.23 SNR obtained by Hamming filter with different cof in water. 64

Figure 3.24 Transverse image when reconstructed using Hamming filter scanning in water. 64

Figure 3.25 Contrast obtained by Hanning filter with different cof in water. 65

Figure 3.26 SNR obtained by Hanning filter with different cof in water. 65

Figure 3.27 Transverse image when reconstructed using Hanning filter scanning in water. 66

Figure 3.28 Contrast for Butterworth filter with order 5 and cof 0.35 Nq (default filter) in water. 67

Figure 3.29 SNR for Butterworth filter with order 5 and cof 0.35 Nq (default filter) 67

Figure 3.30 Transverse image when reconstructed using default filter scanning in water. 68

Figure 3.31 Contrast for Butterworth filter with order 8 and different cof. 68

Figure 3.32 SNR for Butterworth filter with order 8 and different cof. 69

Figure 3.33 Transverse image when reconstructed using Hanning filter scanning in water. 69

Figure 3.34 Contrast for Butterworth filter with order 16 and different cof in water. 70

Figure 3.35 SNR for Butterworth filter with order 16 and different cof in water. 71

Figure 3.36 Transverse image when reconstructed using Butterworth filter order 8 scanning in wate 71

Figure 3.37 Contrast for Butterworth filter with order 24 and different cof in water. 72

Figure 3.38 SNR for Butterworth filter with order 24 and different cof in water. 73

Figure 3.39 Transverse image when reconstructed using Butterworth filter order 24 scanning in water. 73

Figure 3.40 Contrast for Butterworth filter with order 32 and different cof in water. 74

Figure 3.41 SNR for Butterworth filter with order 32 and different cof in water. 74

Figure 3.42 Transverse image when reconstructed using Butterworth filter order 32 scanning in water. 75

Figure 3.43 Contrast for Gaussian filter with order 7 and different cof in water. 76

Figure 3.44 SNR for Gaussian filter with order 7 and different cof in water. 77

Figure 3.45 Transverse image when reconstructed using Gaussian filter order 7 scanning in water. 77

Figure 3.46 Contrast for Gaussian filter with order 14 and different cof in water. 78

Figure 3.47 SNR for Gaussian filter with order 14 and different cof in water. 79

Figure 3.48 Transverse image when reconstructed using Gaussian filter order 14 scanning in water 79

Figure 3.49 Contrast for Gaussian filter with order 21 and different cof in water. 80

Figure 3.50 SNR for Gaussian filter with order 21 and different cof in water. 81

Figure 3.51	Transverse image when reconstructed using Gaussian filter order 21 scanning in water.	81
Figure 3.52	Contrast for Gaussian filter with order 28 and different cof in water.	82
Figure 3.53	Contrast for Gaussian filter with order 28 and different cof 0.2 in water.	83
Figure 3.54	Transverse image when reconstructed using Gaussian filter order 28 scanning in water.	83
Figure 3.55	Contrast for Ramp filter in radioactive medium.	84
Figure 3.56	SNR for Ramp filter in radioactive medium.	84
Figure 3.57	Transverse image when reconstructed using Ramp filter scanning in radioactive medium	85
Figure 3.58	Contrast image for Parzen filter with different cof in radioactive medium.	86
Figure 3.59	SNR for Parzen filter with different cof in radioactive medium.	86
Figure 3.60	Transverse image when reconstructed using Parzen filter scanning in radioactive medium	87
Figure 3.61	Contrast image for Hamming filter with different cof in radioactive medium.	88
Figure 3.62	SNR for Hamming filter with different cof in radioactive medium.	88
Figure 3.63	Transverse image when reconstructed using Hamming filter scanning in radioactive medium.	89
Figure 3.64	Contrast image for Hanning filter with different cof in radioactive medium.	90
Figure 3.65	SNR for Hanning filter with different cof in radioactive medium.	90
Figure 3.66	Transverse image when reconstructed using Hanning filter scanning in radioactive medium	91
Figure 3.67	Contrast image for Butterworth filter with order 5 and cof 0.35 (default filter) in radioactive medium.	92
Figure 3.68	SNR image for Butterworth filter with order 5 and cof 0.35 (default filter) in radioactive medium.	92
Figure 3.69	Transverse image when reconstructed using Butterworth filter order 5, cof 0.35 Nq scanning in radioactive medium	93

Figure 3.70	Contrast image for Butterworth filter with order 8 and different cof in radioactive medium.	93
Figure 3.71	SNR image for Butterworth filter with order 8 and different cof in radioactive medium.	94
Figure 3.72	Transverse image when reconstructed using Butterworth filter order 8 with different cof scanning in radioactive medium	95
Figure 3.73	Contrast image for Butterworth filter with order 16 and different cof in radioactive medium.	96
Figure 3.74	SNR for Butterworth filter with order 16 and different cof in radioactive medium.	96
Figure 3.75	Transverse image when reconstructed using Butterworth filter order 16 with different cof scanning in radioactive medium	97
Figure 3.76	Contrast image for Butterworth filter with order 24 and different cof in radioactive medium.	98
Figure 3.77	SNR for Butterworth filter with order 24 and different cof in radioactive medium.	98
Figure 3.78	Transverse image when reconstructed using Butterworth filter order 24 with different cof scanning in radioactive medium	99
Figure 3.79	Contrast image for Butterworth filter with order 32 and different cof in radioactive medium.	100
Figure 3.80	SNR for Butterworth filter with order 32 and different cof in radioactive medium.	100
Figure 3.81	Transverse image when reconstructed using Butterworth filter order 32 with different cof scanning in radioactive medium	101
Figure 3.82	Contrast image for Gaussian filter with order 7 and different cof in radioactive medium.	102
Figure 3.83	SNR for Gaussian filter with order 7 and different cof in radioactive medium.	102
Figure 3.84	Transverse image when reconstructed using Gaussian filter order 7 with different cof scanning in radioactive medium	103
Figure 3.85	Contrast image for Gaussian filter with order 14 and different cof in radioactive medium.	104
Figure 3.86	SNR image for Gaussian filter with order 14 and different cof in radioactive medium.	104

Figure 3.87	Transverse image when reconstructed using Gaussian filter order 14 with different cof scanning in radioactive medium	105
Figure 3.88	Contrast image for Gaussian filter with order 21 and different cof in radioactive medium.	106
Figure 3.89	SNR for Gaussian filter with order 21 and different cof in radioactive medium.	107
Figure 3.90	Transverse image when reconstructed using Gaussian filter order 14 with different cof scanning in radioactive medium	107
Figure 3.91	Contrast image for Gaussian filter with order 28 and different cof in radioactive medium.	108
Figure 3.92	SNR for Gaussian filter with order 28 and different cof in radioactive medium.	108
Figure 3.93	Transverse image when reconstructed using Gaussian filter order 14 with different cof scanning in radioactive medium	109
Figure 3.94	Percentage of contrast difference between without and with physical filters	112
Figure 3.95	Percentage of SNR difference between without and with physical filters.	114
Figure 3.96	A tranverse slice of phantoms with and without physical filter.	115
Figure 3.97	Percentage of volumre difference between the true and the measured size using no physical filters and with physical filters for different size.	117
Figure 3.98	Percentage of total activity difference between true and measured total activity using no physical filters and with physical filters	119

LIST OF PLATES

		Page
Plate 2.1	ADAC Forte gamma camera with 2 detectors.	29
Plate 2.2	Pegasys Image Processing & Display Workstation	31
Plate 2.3	LEHR collimator mounted on the detector	32
Plate 2.4	A series of syringe as small cylinders.	32
Plate 2.5	Cylindrical water tank phantom.	33
Plate 2.6	Tc-99m generator.	34
Plate 2.7	Tc-99m inside lead elution bottle.	34
Plate 2.8	Cu as physical filter	35
Plate 2.9	Rotation of detector to obtain 64 views	37
Plate 2.10	Image display for ROI Analysis application	42

LIST OF ABBREVIATIONS

Al	Aluminium
ADC	Analog-data-converter
Ci	Curie
cm	centimetre
cof	Cut-off frequency
CRT	Cathode ray tube
Cu	copper
CW	Compton window
DAS	Data acquisition system
FBP	Filtered-back projection
fig	Figure
FOV	Field of view
GLH	Gray Level Histogram
keV	Kilo electron volt
LEHR	Low Energy High Resolution
mCi	milicurie
ml	mililitre
mm	milimetre
Na	Natrium (sodium)
Nq	Nyquist
Pb	Plumbum (lead)
PHA	Pulse Height Analyzer

PMT	Photo multiplier tube
PSRF	Point-spresd response function
ROI	Region of interest
Sn	Stanum (tin)
SNR	Signal-noise ratio
SPECT	Single Photon Emission Computed Tomography
TEW	Triple Energy Window
Tl	Thallium
Tc-99m	Technitium-99 metastable
Zn	Zinc
3D	Three dimension

LIST OF SYMBOLS

γ	gamma
%	percentage
μ	mikro

KESAN PENURAS DIGITAL DAN FIZIKAL TERHADAP KUALITI IMEJ BAGI PENGIMEJAN KUANTITATIF Tc-99m PANCARAN FOTON TUNGGAL TOMOGRAFI BERKOMPUTER (SPECT)

ABSTRAK

Pengukuran kuantitatif dilakukan menggunakan data SPECT untuk mengukur saiz dan menganggar jumlah aktiviti radionuklid di dalam sesuatu organ atau lesi. Foton terserak pada imej merupakan masalah utama untuk memperolehi pengukuran kuantitatif yang tepat. Tujuan kajian ini dilakukan adalah untuk mengkaji kesan penuras fizikal terhadap kualiti imej di dalam pengimejan kuantitatif SPECT. Dua jenis penuras fizikal iaitu kuprum (Cu) dengan ketebalan 0.05 cm dan aluminium (Al) dengan ketebalan 0.04 cm (aluminium A) dan 0.06 cm (aluminium B) digunakan sebagai kaedah pembetulan sinaran terserak. Enam penuras matematikyang berlainan termasuk Ramp, Parzen, Hanning, Hamming Butterworth dan Gaussian dengan berlainan ‘order’ dan had frekuensi (cof) digunakan di dalam pemprosesan imej**.** Imej fantom diperolehi dengan menggunakan kolimator tenaga rendah-resolusi tinggi, tetingkap simetri untuk tenaga 126 hingga 154 keV (140 keV adalah titik tengah). 64 projeksi / 360^0 dan 30 saat/projeksi, jarak radius pusingan adalah 30 cm dari fantom dengan matrix 64 x 64 x 16. Perbezaan pembilangan di dalam imej sebelum dan selepas pemprosesan imej menggunakan Ramp, Gaussian dan Butterworth adalah tidak bergantung kepada saiz fantom. Perbezaan pembilangan di dalam imej bagi Parzen, Hamming dan Hanning bergantung kepada saiz bagi saiz fantom yang kecil (10 ml, 20 ml, 30 ml dan 40 ml). Penurunan pembilangan di dalam imej bertambah apabila cof ditingkatkan bagi penuras Parzen, Hamming, Hanning, Gaussian dan Butterworth . Kontras dan nisbah isyarat –hingar (SNR) meningkat apabila saiz fantom dan cof bertambah bagi kesemua penuras matematik. Penggunaan penuras fizikal yang spesifik tidak sesuai untuk saiz fantom yang berlainan bagi meningkatkan kontras dan SNR. Ketepatan anggaran saiz fantom tanpa menggunakan penuras fizikal adalah 5.3 ± 16.5 %, 13.1 ± 46.7 % untuk Cu, 4.7 ± 38.6 % untuk aluminium A dan aluminium B adalah 8.6 ± 38.5 %. Penggunaan penuras fizikal akan memberikan anggaran saiz fantom yang terlebih besar bagi fantom bersaiz kecil dan anggaran saiz fantom yang terlebih kecil bagi fantom bersaiz besar (70 ml, 130 ml dan 170 ml) berbanding tanpa penggunaan penuras fizikal. Ketepatan anggaran jumlah aktiviti adalah -49.3 ± 10 % tanpa menggunakan penuras fizikal,- 48.9 ± 16.6 % bagi Cu, , -55.6 ± 16.6 % untuk aluminium A and -55.5 ± 13.4 % untuk aluminium B. Anggaran jumlah aktiviti adalah kurang berbanding nilai sebenar samada menggunakan penuras fizikal atau tidak. Anggaran saiz fantom dan jumlah aktiviti yang lebih tepat dapat diperolehi tanpa penggunaan penuras fizikal.

THE EFFECT OF DIGITAL AND PHYSICAL FILTERS ON IMAGE QUALITY FOR QUANTITATIVE Tc-99m SINGLE PHOTON EMISSION COMPUTED TOMOGRAPHY (SPECT)

ABSTRACT

An absolute quantitation can be made on SPECT data to accurately measure the volume and estimate total radionuclide activity in the organ or lesion. The major problem to produce an accurate quantitation is the contamination of SPECT images by scattered photons. The aim of the study is to investigate the effect of physical filters on image quality in quantitative SPECT imaging. Two types of material filters viz copper (Cu) with 0.05 cm thickness and aluminium (Al) with 0.04 cm (aluminium A) and 0.06 cm thickness (aluminium B) were applied as scattered radiation correction method. Six different mathematical filters such as Ramp, Parzen, Hanning, Hamming, Butterworth and Gaussian filter with different order and cut-off frequency (cof) were used to reconstruct the images. The image for each phantom was acquired by using low-energy-high-resolution (LEHR) collimator, symmetrical window of 126 to 154 keV (centered at 140 keV), 64 views over 360^0 and 30 seconds/projection. The radius of rotation was 30 cm from the phantom with 64 x 64 x 16 matrix. The image count difference between before and after reconstruction using Ramp (76 to 78 %), Gaussian and Butterworth filters were independent of the size of the phantoms. Parzen, Hanning and Hamming showed an image count dependency on size for small phantom sizes (10 ml, 20 ml, 30 ml and 40 ml). As cof increased the image count reduction increased. Contrast and signal-noise ratio (SNR) increased when the sizes of phantoms and cof increased for all mathematical filters. Using specific physical filter does not suit different sizes of phantom for contrasts and SNR improvement. The accuracy of volume estimation when not using physical filter is 5.3 ± 16.5 %, 13.1 ± 46.7 % for copper, 4.7 ± 38.6 % for aluminium A and aluminium B is 8.6 ± 38.5 %. Using physical filters give extreme overestimation of the true volume for small phantoms and underestimation for big phantoms (70 ml, 130 and 170 ml) compared to without using material filters. Accuracy for total activity determination is -49.3 ± 10 % without using physical filters, -48.9 ± 16.6 % for copper, -55.6 ± 16.6 % for aluminium A and -55.5 ± 13.4 % for aluminium B. Total activity determination is underestimated either using physical filter or not. The best accurate of volume estimation and total activity determination is obtained without using physical filters.

CHAPTER I
INTRODUCTION

1.1 Single Photon Emission Computed Tomography (SPECT)

Single Photon Emission Computed Tomography is one of the special techniques in nuclear imaging to image and analyze radiopharmaceutical distribution in human body using gamma camera. The advantages of SPECT imaging over the conventional nuclear scanning are its ability to produce three-dimensional images of radiopharmaceutical within the body and improve image quality. The three-dimensional localization in the various tissue of the body could give crucial information related to physiological process in both healthy and diseased tissue.

Basically in SPECT imaging the gamma photon emitted from the decaying process of the radionuclide inside the body will be detected at discrete angle around the patient at 180^0 or 360^0 angular sampling as shown in fig. 1.1. The data will be collected at each angle and stored in the computer system for reconstruction of transverse, sagittal and coronal images.

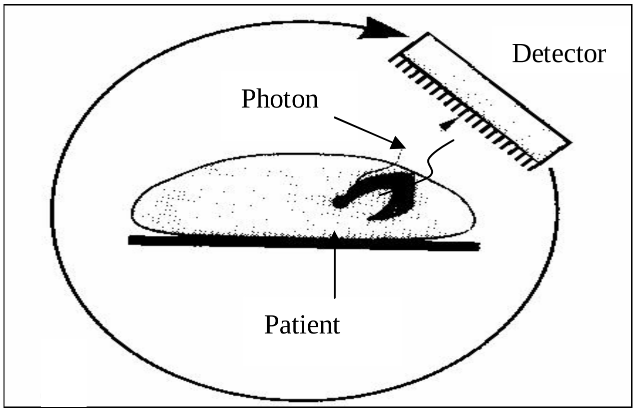

Figure 1.1: A schematic diagram showing the detection of photons emitted from the radionuclide in the body.

1.2 Principle of gamma camera

The gamma camera or Anger scintillation camera was invented by Hal Anger of Donner Laboratory, University of California in the late 1950's. Basically, it comprises of lead collimator, sodium iodide (NaI(Tl) scintillation crystal, photomultiplier tube (PMT), pulse height analyzer (PHA), cathode ray tube (CRT) display and control console.

According to figure 1.2, the detection of the radiation begins when the gamma (γ) photons emitted from the source passing through a hole in the collimator and detected by NaI(Tl) scintillation crystals. Simultaneously, the crystals will convert the photons into light pulses and subsequently into voltage signals by an array of PMT. The signal is then processed by PHA to discriminate the events occurred whether to be stored and display at the CRT or need to be rejected. Apparently, pulse height analyzer (PHA) in the system is to select only the energy desired by setting the appropriate peak and window in order to reduce the amount of scattered radiation recorded. While, the console control function is to adjust the setting of the parameter desired such as position the PHA window or energy window, duration of the imaging time and manipulate the CRT image displayed.

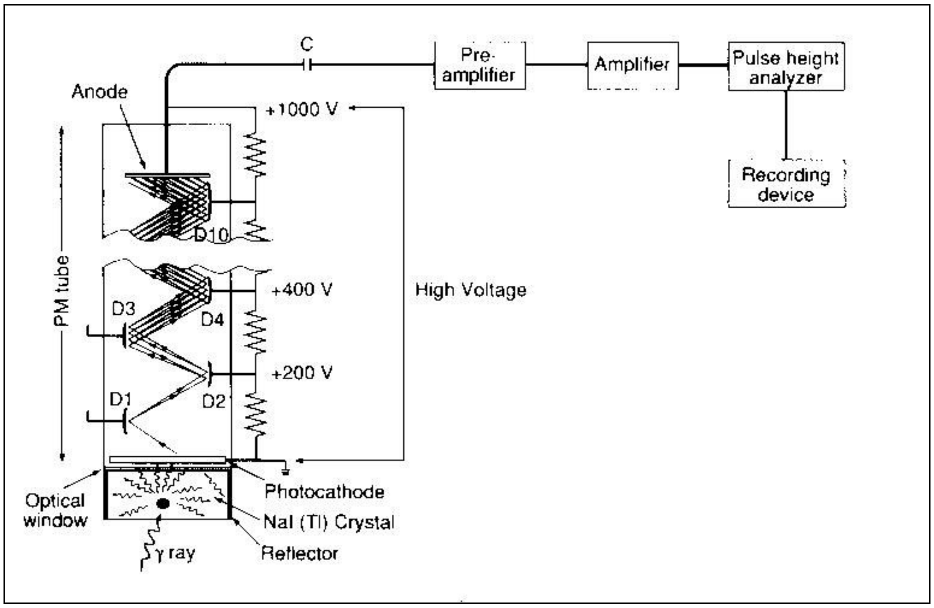
C
Pre-amplifier
Amplifier
Pulse height analyzer
Recording device
Anode
+1000 V
PM tube
D10
+400 V
High Voltage
D3
D4
+200 V
D1
D2
Optical window
Photocathode
NaI (Tl) Crystal
Reflector
γ ray

Figure 1.2 : Schematic representation showing a conversion of γ-rays to voltage signals in gamma camera system

1.3 SPECT image reconstruction

The filtered-backprojection (FBP) method is the most popular technique to reconstruct SPECT image. This technique is performed by applying a 'filter' in simple backprojection method.

1.3.1. Simple Backprojection

The basic principle of this method is shown in figure 1.3 below. In A, an object of two hot spots is viewed with 3 detectors around it to collects the data. The analog data projection are received and transferred by the data acquisition system (DAS) to the analog-data-converter (ADC) to become a digital image projection. Reconstruction is carried out by allotting each pixel count of a given projection in the acquisition matrix to all pixels along the line of collection in the reconstruction matrix (figure B). When many projections are backprojected, an image in figure C will be produced.

However, simple backprojection has the problem of image blurring because of ‘star pattern’ artefacts. This blurring effect can be minimized by applying a ‘filter’ to the acquisition data and then backprojected to produce an image which is more similar to the original object.

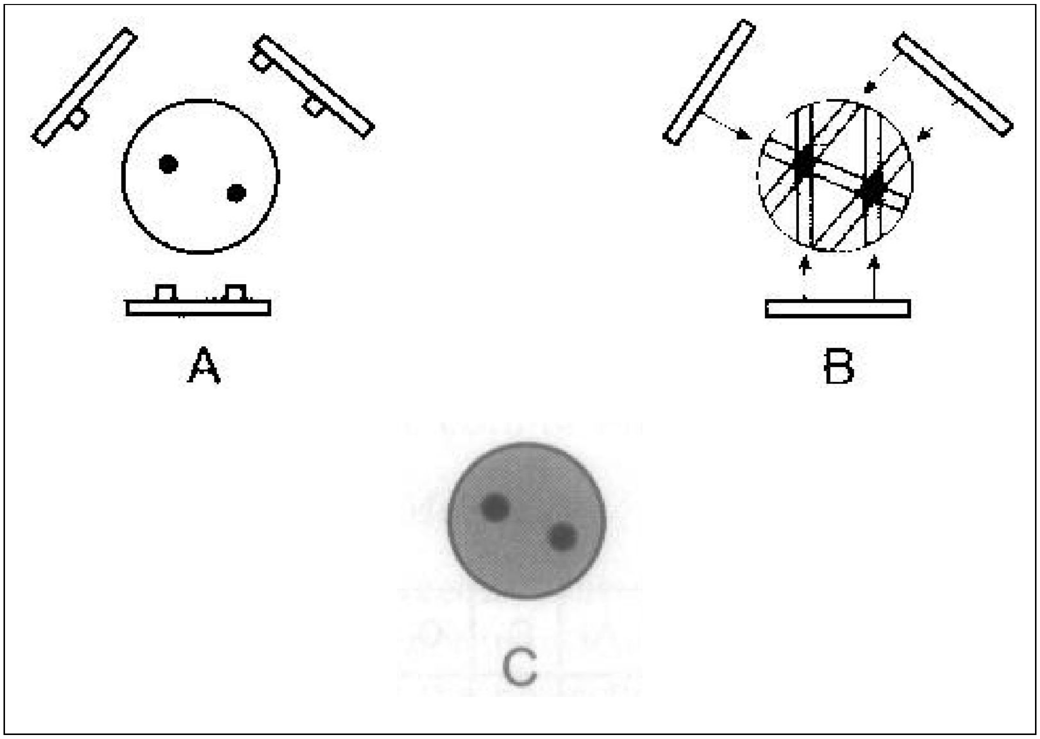

Figure 1.3: Basic principle of reconstruction technique by backprojection technique *(Resource:Physics and Radiobiology of Nuclear Medicine)*

1.3.2 Filtered-backprojection (FBP)

This technique is performed by applying a ‘filter’ in simple backprojection method. One of the most filtered-backprojection is the Fourier method. The Fourier method of filtering basically based on transformation of projection data from the spatial domain to the frequency domain by using ramp filter and expressed as:

$$F(v_x, v_y) = \mathcal{F} f(x,y) \qquad (1)$$

where $F(v_x,v_y)$ denotes the Fourier transform of $f(x,y)$ and F represents Fourier transformation. Then, for a Fourier filter, H(v) is applied in the frequency domain as follow:

$$F'(v) = H(v).\ F(v) \tag{2}$$

where F'(v) is the filtered backprojection in the frequency domain. Finally, the inverse Fourier transformation is performed to change the frequency domain to spatial domain which means the filtered projections is backprojected.

1.4 SPECT reconstruction filter

Basically, filtering is the term used for any operation that applied to pixels in an image. This is includes smoothing, edge detection enhancement and resolution recovery in order to extract important and relevant information within nuclear medicine images.

A well-known and common filter is the ramp filter. The formula of this filter is:

$$R(f) = f \tag{3}$$

Where R(f) is the ramp filter and f is the frequency increments. The graphical representation for equation (3) is given in fig. 1.4 .

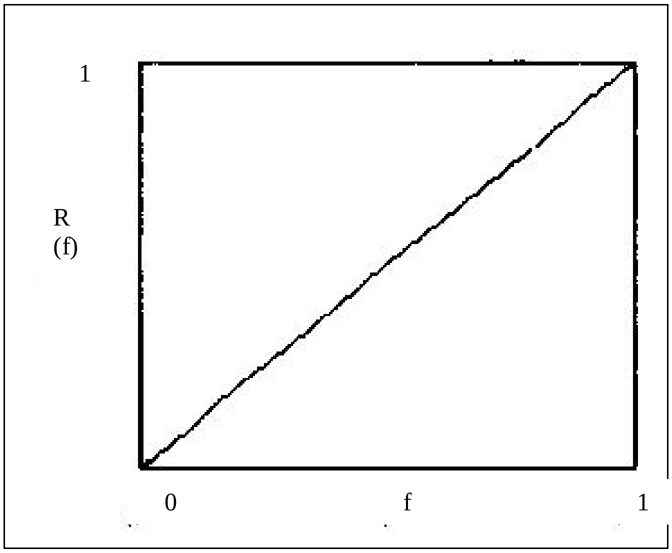

Figure 1.4: Ramp filter function *(Resource : SPECT A primer)*

Ramp filter will suppress the background noise exists in the low frequency range that contribute a smoothing or blurring effect in the final reconstruction. Subsequently, the ramp filter will accept only a data above a specified frequency and excluding the low frequency as shown in figure 1.5 (English, 1995).

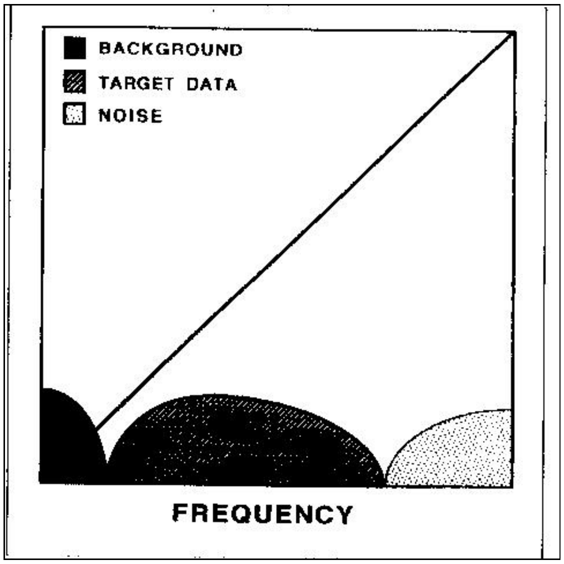

Figure 1.5: The ramp filter removes background noise at low frequency and accept useful image data and high noise. *(Resource : SPECT A primer)*

Another types of digital filters has been designed including Shepp-Logan, Hamming, Hanning and Parzen which corresponds to their respective designer. These filters are also known as 'low pass' filters as they preserve low frequency structures and eliminate high frequency noise. The filters are defined by fixed formula with frequency, f and user-selected cut-off frequency, n as given by equations (4) – (7) and as figure 1.6 respectively (Saha, 2001).

Shepp-Logan, $SL(f) = \sin(\pi f)^{2n}/(\pi f/2n)$ (4)

Hamming, $Hm(f) = 0.54 + 0.46 \cos(\pi f/n)$ (5)

Hanning, $Hn(f) = 0.5 + 0.5 \cos(\pi f/n)$ (6)

Parzen, $P(f) = f\,[2(1 - 3\,(f/n)]$ (7)

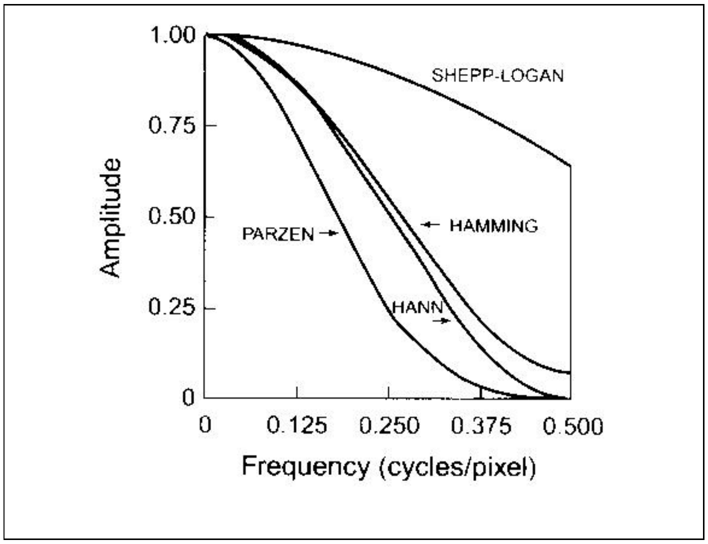

Figure 1.6: Different windows suppress the high frequencies with a cut-off Nyquist frequency of 0.5 cycle/pixel. *(Resource : Physics and Radiobiology of Nuclear Medicine)*

The disadvantage of using the ramp filter only is that it amplifies the noise at high frequency. To avoid this problem, the window filter is always used which is the combination between Ramp filter and 'low pass' filters to produce an optimal image quality which is the trade-off between contrast and resolution. Fig. 1.7 shows the combination filter function between Ramp filter and 'low pass' filters.

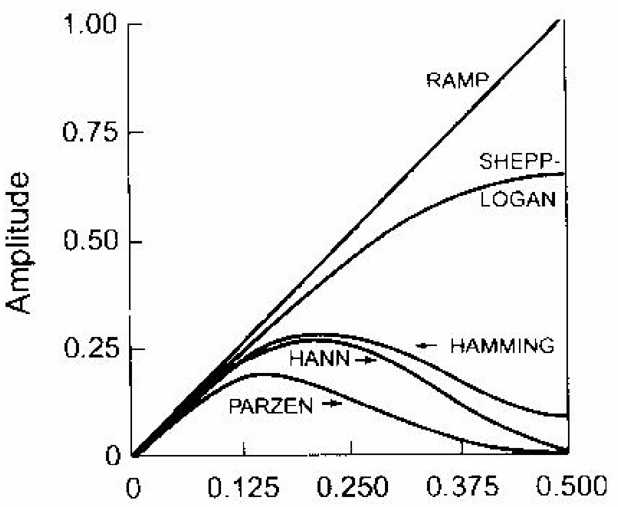

Figure 1.7: Different windows by multiplying respective filters with the Ramp filter.

The cut-off frequency defines at which the frequency accepted and the frequency above the band will be eliminated (Saha, 2001, Van Laere *et al.*, 2001).

The most frequently used filter in nuclear medicine is the Butterworth filter. The formula is as below (Saha, 2001):

$$\text{Butterworth, } Bu(f) = 1/\ 1 + (f/v_c)^{2n} \qquad (8)$$

This filter is characterised by 2 parameters, the cut-off frequency, v_c and the order, n. Regarding to fig. 1.8, the cut-off frequency in Butterworth filter is the frequency at which the amplitude is attenuated and not the frequency which it is eliminated as other filters (Saha

2001). Meanwhile, the order determine how rapidly the attenuation of amplitude occurs by changing the slope of the filter function (Saha, 2001, Van Laere *et al.*, 2001). Order with high value will produce sharp fall and allows to retain the contrast while still eliminating noise at high frequencies.

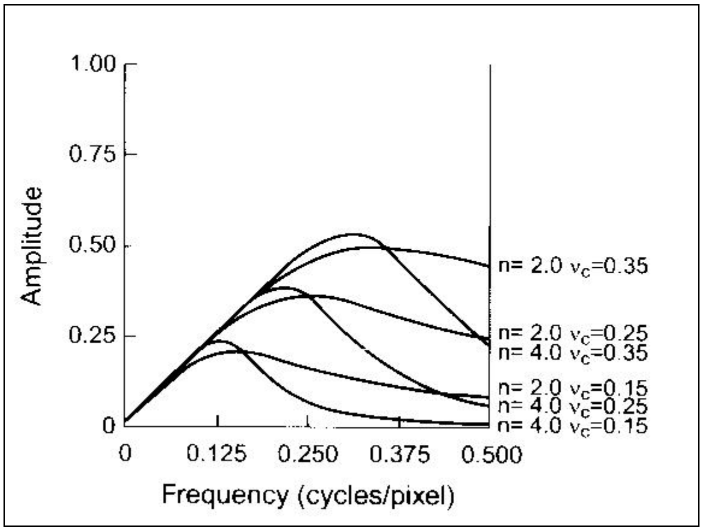

Figure 1.8: Butterworth filter multiply with Ramp filtes with different orders, n and cutoff frequencies, v_c

1.4.1 Nyquist frequency

Nyquist frequency is a maximum frequency that gives upper limit to the number of the frequency necessary in each pixel to represent an image projection. This term is used to characterize the digital filters that have been designed and applied to reconstruct the images. Since the frequency is the sine and cosine curve, it means 1 cycle needs at least 2 pixels to be completed. The value of Nyquist frequency is 0.5 cycle/pixel.

1.5 LITERATURE REVIEW

1.5.1 SPECT Quantification

There are possible benefits of using quantitative SPECT imaging in radiology, cardiology, neurology and oncology. For example, the application of monoclonal antibody imaging for diagnosis or treatment (Pollard *et al.*, 1992). The necessary dose needed of monoclonal antibodies could be obtained by quantifying the target-to-injection dose ratio and the activity concentration in the region.

The developments of labelled drug in cancer chemotherapy have an advantage to predict tumour response to therapy and the exact amount of dose given for better treatment. It has been achieved by calculating the drug uptake by lesion using quantitative SPECT data (Even-Sapir *et al.*, 1994, Front *et al.*, 1987b). This treatment response obtained is very useful in planning further treatment for individual cancer patients.

When using radiation as cancer treatment, the effective dose of radiation should be administered for successful treatment to avoid any occurrence of unwanted biological effects. Previously, assumption was made that the amount of drug administered is directly depicted by the amount of drug delivered to the tumour. When using SPECT, it is clear that the quantity of drug delivered is not essentially related to the amount administered (Israel *et al.*, 1990, Iosilevski *et al.*, 1989). Therefore, the amount of dose could be calculated using quantitative SPECT data after considering the lesion volume, the activity concentration and the absorbed dose to alter the the dose scheduling.

The quantitative SPECT method also has been applied to predict the bone metabolism in hyperthyroidism and thyrotoxicosis (Israel *et al.*, 1991). It can also identify radiation effect to bone metabolism (Israel *et al.*, 1992). The study was then continued to determine bone loss in hyperparathyroidism (Israel *et al.*, 1998) and in renal disease (Israel *et al.*, 1995). By using this valuable method, the threshold dose for treatment response of bone metastatic disease was found as well (Israel *et al.*, 2000).

Measurement of myocardial volume (Caputo *et al.*, 1985) and mass (Corbett *et al.*, 1984) using quantitative SPECT data has positive implication in evaluating cardiac function. According to the results of these studies, it has been proved that this non-invasive quantitative technique is accurate and clinically applicable.

Other examples of the application of quantitative SPECT include the detection of liver cirrhosis and evaluation of the severity of the disease (Groshar *et al.*, 2002), distinguishing lymphoma from benign hilar (Even-Sapir *et al.*, 1995), measurement of liver and spleen volume (Strauss *et al.*, 1984), kidney volume (King *et al.*, 1998) and thyroid volume (Zaidi, 1996b).

An absolute quantification can be made using SPECT data to accurately measure the area or volume of an organ or lesion. In addition, this quantitative SPECT technique can also estimate the concentration or total of radionuclide activity in lesion or organ of interest.

Changes of organ/lesion size and uptake give a significantly clue to the presence of disease. It also depicts the response in a therapy, thereby indicating a success or failure of the treatment. Therefore by estimating the organ/lesion volume and activity concentration, one can quantitatively differentiate the infection from healthy region and treatment outcome can be monitored as well. From the total activity obtained, the absorbed dose for region of interest could be determine in order to estimate the effective dose given for effective treatment.

However, accurate quantitation of SPECT is hampered by some of the physical factors including photon attenuation and scattering. Contamination of images by scattered photons is the major hindrance in quantitative SPECT (Floyd *et al.*, 1988). The scattered radiation affects the contrast and resolution of images. Even though the conventional scatter correction method can improve radioactivity quantification, it still unable to accurately increase lesion detection significantly (de Vries *et al.*, 1999). When photon attenuation and scattering are not corrected, then the organ/lesion volume calculation could not be accurately determined.

1.5.2 Image segmentation and boundary detection

Accurate determination of organ volumes is important for measurement of radionuclide activity. The quantification of organ volumes from SPECT images is influenced by image segmentation and system transfer function. Image segmentation defines the boundary of an organ and volumes can be determined by total number of voxels contained within the defined edge and multiplied by the size of one voxel.

The operator-drawn region of interest is the simplest method to define edge of an organ image. The organ or uptake region in a section image will be outlined by the trained observer to create region of interest (ROI). By using this method, the volume of organ or region is calculated by summing up total number of voxel in each ROI and each slice. However this method has poor precision and depends solely on the operator (Macey and Giap, 1995).

Another approach is fixed count threshold. In this method, the background counts from each voxel are removed by trilinear interpolative correction. After that, the remaining counts are compared with a count threshold, typically 50 % of the maximum count to define the edge.

A threshold of 50 % is expected to give the best estimation of boundary location due to the absence of background activity, attenuation and scatter in addition to assuming an activity distribution in the object is uniform and spatial resolution is reasonable (Long *et al.*, 1992). However, the best threshold depends on the background activity, the source size and shape relative to the spatial resolution of the imaging system (King *et al.*, 1991)

The gray-level histogram (GLH) method is an adaptive threshold method. It uses nonparametric procedure of automatic threshold selection instead of using a universal fixed threshold to separate object and background pixels. A count threshold that maximizes the separability of object and background in the GLH is determined. The advantage of this method that it is semiautomatic and virtually operator independent (Mortelmans *et al.*, 1986)

Another image segmentation method is the gradient-based edge detection method (Long *et al.*, 1991). It is based on calculation of the gradient for the number of counts in each voxel of a section image. The gradient is the magnitude and direction of the rate of change in count in each voxel in relation to adjacent voxel. The matrix is then searched for local maximum of gradient magnitude to determine candidate edge voxel. The edge voxels are selected among the candidate edge voxels based upon an adaptive thresholding of both gradient magnitude and voxel count. This is followed by filling in the region enclosed by the edge voxels for each slice. The total number of voxels enclosed in the ROI is multiplied by the unit volume of a voxel to yield volume. This method is automatic, reproducible, and outlines edge rapidly with minimal operator intervention.

The boundary detection using 90^0 Compton Scattered photon was developed by Macey *et al.* (1988). It uses a collimated ^{99m}Tc line source located outside the transverse section image at a 90^0 angle to the direction of view for the collimator. A 20 % window at 110 keV is set to record scattered photon. In phantom studies, an accuracy of 6 mm was reported in the location of the boundary of a 22-cm diameter cylindrical phantom.

1.5.3 Attenuation correction

Attenuation is the loss of photon counts either by absorption in the medium or by scattering outside the field of view of the detection system. Therefore, some photons will not be detected or will be recorded as misplaced events. This problem could degrade the image quality and ambiguously detect the location of lesion.

Generally, the attenuation correction methods can be categorized into three groups which are pre-processing method, intrinsic method and post processing method. With an assumption that the radioactivity within the body is uniformly distributed and the attenuation coefficient is constant for the whole body, the pre-processing methods involves mathematical development based on geometric mean and arithmetic mean of conjugate projection view of images and applied before reconstruction (Macey and Giap, 1995). The geometric mean tend to give count density between isolated radioactive source while the arithmetic mean will shows reduction in count density towards the centre of the reconstructed image. However in clinical case, the radioactivity of radiopharmaceutical is not uniformly distributed due to the different uptake of the lesion and each organ attenuates photon differently.

Intrinsic method involves multiplying the projection data with an exponential function during reconstruction process. The exponential function is the function of body thickness. It can work with multiple source and simple to implement. However, it also amplify noise onto the reconstructed image and application of smoothing filter is suggested to control the noise (Rosenthal *et al.*, 1995).

The post processing method proposed by Chang (1978) corrects the attenuation by multiplying each pixel counts in the image with a correction factor after image reconstruction. A correction factor is calculated at each image point as the average attenuation factor for all projection angles. But, this compensation method could overcorrect or under correct some part of the image. Because of this, an iteration of this method is recommended to improve the compensation (Rosenthal *et al.*, 1995).

1.5.4 Scattered Radiation Correction

When photon interacts with matter, scattering will occur. There are two types of scattering that need to be considered, coherent and incoherent (Compton) scattering.

Coherent scattering involves an interaction of a photon with an atom but there is no loss of energy. Usually it comprises only a small change in direction for incoming photons. This type of scattering can be included in the primary photons and there is no need to correct them (Zaidi and Koral, 2004). In addition, their occurrence is much less than Compton-scattered photons.

In coherent or Compton scattering, interaction of photons with matter will lose some energy and changes its initial direction. And this is the main cause of photon scattering in tissue (Beekman *et al.*, 2001). When the original direction of incoming photons is changing, it will be scattered either in the patient or the collimator and detected back incorrectly as it is from emission site. This phenomenon contributes the major problem that need to be corrected such as contrast degradation, haziness and loss in quantitative accuracy (Bouwens *et al.*, 2001).

One way to decrease the detection of scattered photons is to reduce the width of the energy window of PHA. But the number of the primary photons will be decreased thus increasing the noise level. Besides, NaI(Tl) systems cannot reject all scatter and the rejection becomes more difficult for gamma ray below about 200 keV, as shown in fig. 1.9 (Sorenson and Phelps, 1980). The higher the energy of the photopeak, the scattered radiations are widely distributed at lower energy. Thus, in this case the elimination of scattered radiations becomes easier as the radiation is not overlapped at the photopeak energy.

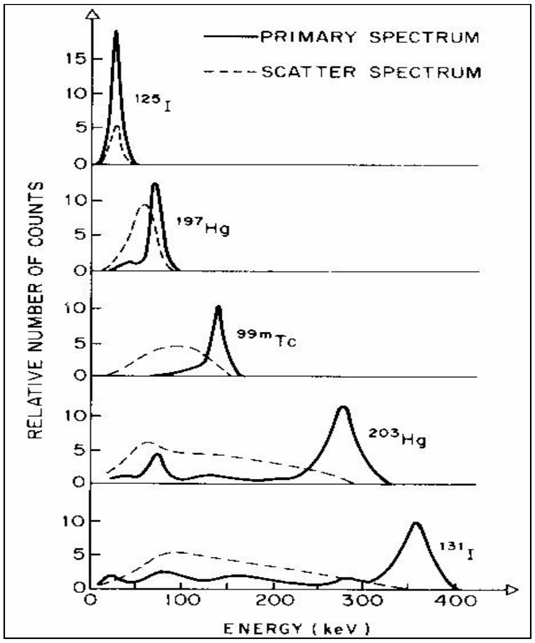

Figure 1.9: The figure shows the different primary and scatter spectrum energy of different radioactive *(Resource: Physics in Nuclear Medicine)*

Koral *et al.* (1988) have investigated the scatter correction by analysing the energy spectra. This spectral fitting method involves establishing the shape of the scatter-free spectrum. The hypothesis is the complete energy spectrum at various spatial locations in SPECT projection images can be analyzed to separate the Compton-scattering from the unscattered component. After analyzing the spectrum, the amount of Compton-scattering at each location is obtained and used in correcting the 3-dimensional projection image. To analyze the spectrum, the shape of the Compton-scattering was represented by:

$$c_i = a_o + a_1 i + a_2 i^2 + a_3 i^3 \qquad (9)$$

where c_i is the number of counts in an energy bin, i is the bin number and a_o, a_1, a_2 and a_3 are parameters to be determined from the fitting. For nonscattered spectrum, the shape was given by:

$$d_i = bf_i \qquad (10)$$

where d_i is nonscattererd spectrum, b is another parameter to be found from the fitting and f_i scatter-free source. The total spectrum, $\bar{y}_i$ is obtained by summing up the scattered and unscattered component:

$$\bar{y}_i = c_i + d_i \qquad (11)$$

The parameters were found by getting the best fit between $\bar{y}_i$ and experimental spectrum, y_i

With the use of a mathematical fitting, the spectrum of scattered photons were obtained by finding the least square fit between the measured spectrum and assumed component. According to the result, the scatter-free spectrums produced have the correct shape as confirmed by simulation study. The method was then validated quantitatively and the results were found to be accurate.

Energy-weighted acquisition method was proposed by Hamill and Devito (1989) for scatter reduction. In essence, the implicit method is based on changing the feature of point-spread response function (PSRF) by designing the weighting function according to different isotopes and collimators. The weighting factor was manipulated experimentally by using the energy spectrum for radionuclide as groundwork. Basically, the factor function is to distribute the events in the image due to the imperfect correlation with an energy signal and the coordinate of point within the patient, (x,y) displacement. By using this energy-weighted, it would reduce scatter tail of PSRF thus the count of scattered photons in a photopeak window for 2-dimensional imaging would be estimated. The measurements show that the function could also reduced the scatter radiation effect by allowing events of all energies to contribute to form an image and improved image contrast.

Another practical method is the triple-energy window approaches which contain three different windows including the photopeak and two subwindows on both side of the main window for scatter subtraction in qualitative SPECT imaging as shown in fig. 1.10. The count acquired with the 2 narrower windows was used to estimate and subtract the count in the main window. First, the total count (C_{total}) in the photopeak window was composed of the count of primary photons (C_{prim}) and scattered photons (C_{scat}). Then, the estimation of the scatter was made from the count data obtained at the two subwindows. The subtraction was then performed at each pixel in each planar image. From the simulation test, the Compton scatters in the main window could be estimated well and the compensated images produced show the agreement with the image produce using primary photons (C_{prim}) (Ogawa *et al.*, 1991).

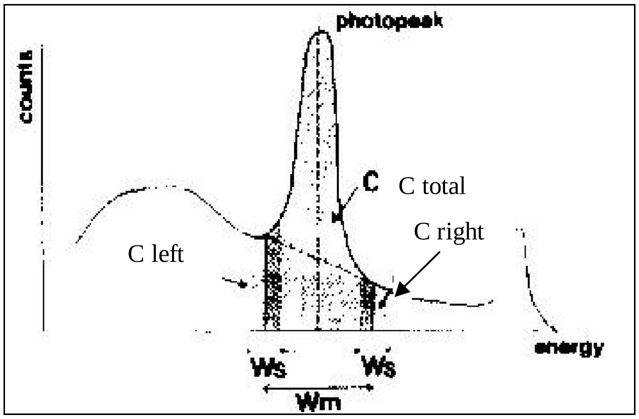

Figure 1.10: C_{total} is the main window while C_{left} and C_{right} are the subwindows located at the end of the main window.

King *et al.* (1992) have developed the dual-photopeak window method for scatter correction. This method consists of the photopeak in the spectrum which was divided into two nonoverlapping energy windows, lower and upper windows which cover the photopeak as shown in fig. 1.11. Hypothesis was made that the lower part of the photopeak contained a significant amount of scatter while the upper region of the photopeak was relatively free from scatter.

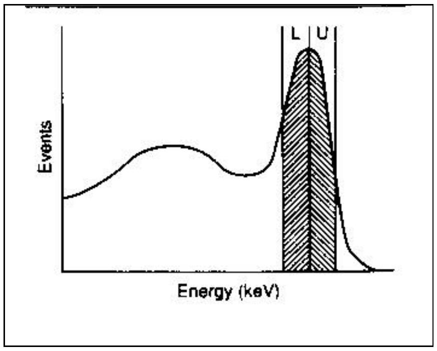

Figure 1.11: Energy spectrum showing location of lower (L) and upper (U) windows used in dual-photopeak window

The scatter fraction, k was determined for scatter compensation method by obtaining the ratio between two energy windows which cover the photopeak. It was represented as:

$$SF = A.\ R_s^{B} + C \qquad (12)$$

where SF is scatter fraction, A, B and C is determined from regression analysis and R_s is the ratio of the corrected counts of the lower window divided by the upper window. Although the application of this method has improved the contrast and quantitative accuracy, in most cases the results still do not match the actual distribution precisely (Buvat *et al.*, 1995) & (Ljungberg *et al.*, 1994).

The other method for scatter correction was the channel ratio method introduced by Pretorius *et al.* (1993). The technique was almost similar to dual-photopeak window but it takes into account the contribution of the scattered photons to the energy spectrum.

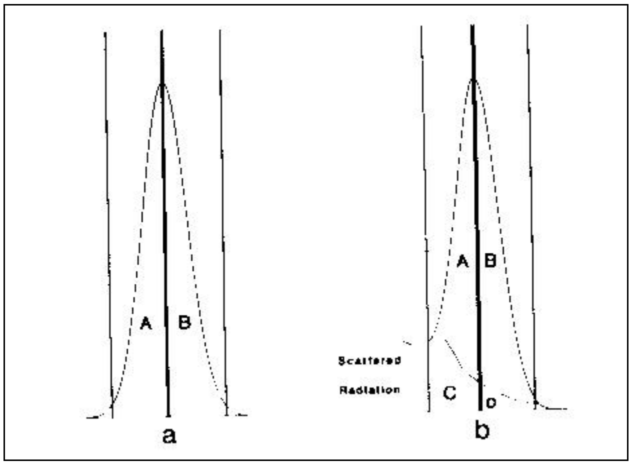

Figure 1.12:a) Placement of windows on the photopeak when no scatter is present.
b) Contribution made by scattered radiation to the photopeak energy windows.